Available online at www.sciencedirect.com
ScienceDirect
Medical Image Analysis 12 (2008) 484–496
MEDICAL IMAGE ANALYSIS
www.elsevier.com/locate/media

Regions, systems, and the brain: Hierarchical measures of functional integration in fMRI

Guillaume Marrelec [a,b,c,*], Pierre Bellec [a,b,d], Alexandre Krainik [e,f], Hugues Duffau [a,b,g], Mélanie Pélégrini-Issac [a,b], Stéphane Lehéricy [h], Habib Benali [a,b,c], Julien Doyon [a,b,c]

[a] *Inserm, U678, Paris F-75013, France*
[b] *Université Pierre et Marie Curie, Faculté de Médecine Pitié-Salpêtrière, Paris F-75013, France*
[c] *Université de Montréal, MIC/UNF, Montreal, Canada H3W 1W5*
[d] *McGill University, MNI, BIC, Montreal, Canada H3A 2B4*
[e] *Inserm, U594, Grenoble F-38000, France*
[f] *CHU La Tronche, Department of Neuroradiology, Grenoble F-38000, France*
[g] *CHU de Montpellier, Hôpital Gui de Chaulic, Montpellier F-34295, France*
[h] *AP-HP, Hôpital Pitié-Salpêtrière, Department of Neuroradiology, Paris F-75013, France*

Received 8 November 2006; received in revised form 17 December 2007; accepted 7 February 2008
Available online 15 February 2008

Abstract

In neuroscience, the notion has emerged that the brain abides by two principles: segregation and integration. Segregation into functionally specialized systems and integration of information flow across systems are basic principles that are thought to shape the functional architecture of the brain. A measure called integration, originating from information theory and derived from mutual information, has been proposed to characterize the global integrative state of a network. In this paper, we show that integration can be applied in a hierarchical fashion to quantify functional interactions between compound systems, each system being composed of several regions. We apply this method to fMRI datasets from patients with low-grade glioma and show how it can efficiently extract information related to both intra- and interhemispheric reorganization induced by lesional brain plasticity.

Keywords: fMRI; Functional brain interactions; Functional connectivity; Integration; Mutual information; Information proper; Multiinformation; Low-grade glioma; Brain plasticity; Surgery

1. Introduction

It has been proposed that functional brain architecture abides by two principles, namely, functional segregation and functional integration (Zeki and Shipp, 1988; Tononi et al., 1998a). While the segregation principle states that some functional processes specifically involve well-localized brain regions, the integration principle acknowledges that even simple behaviors imply the merging of information flows across many systems distributed in the whole brain (Roland and Zilles, 1998; Varela et al., 2001; Passingham et al., 2002). It is only through a subtle balance of these two principles that the brain can efficiently process functional tasks. Segregation and integration have been at the center of much attention in many areas of neuroscience, including theoretical neuroscience and neurocomputing, neuroanatomy, electrophysiology, and functional neuroimaging (for a review, see, e.g., Sporns et al., 2004). The balance between segregation and integration imposes very precise constraints on brain design, granting it with a unique hierarchical structure—neurons, neuron columns, areas, and systems—that, in turn, deeply influences its functional processing at all scales (e.g., Chialvo, 2004). Even though there exists an increasing literature regarding

* Corresponding author. Address: Inserm U678, CHU Pitié Salpêtrière, 91 Boulevard de l'Hôpital, 75634 Paris Cedex 13, France.
E-mail address: marrelec@imed.jussieu.fr (G. Marrelec).

1361-8415/$ - see front matter © 2008 Elsevier B.V. All rights reserved.
doi:10.1016/j.media.2008.02.002

small scale properties of the brain (Buonomano and Merzenich, 1998; Stepanyants and Chklovskii, 2005), most behavioral, imaging, and clinical studies only have access to larger scales, such as areas or systems.

Blood oxygen level dependent (BOLD) functional magnetic resonance imaging (fMRI) is an imaging technique that makes it possible to dynamically and noninvasively follow metabolic and hemodynamic consequences of whole-brain neural activity (Chen and Ogawa, 1999; Huettel et al., 2004). As such, it stands as a potentially powerful candidate for in vivo investigation of functional integration within brain networks. Indeed, it is now increasingly accepted that datasets acquired with that modality convey relevant information relative to functional integration; to what extent such information is available, though, is an issue that remains open and subject to controversies (Stone and Kötter, 2002; Horwitz, 2003; Lee et al., 2003). In fMRI, most approaches to study integration rely on either functional or effective connectivity (for reviews and discussions, see, e.g., Friston, 1994; Marrelec et al., 2006a). The functional connectivity between two voxels or regions is defined as the temporal correlation between the voxel or region time courses (Friston et al., 1993b). As to effective connectivity, it rather considers the influence that regions exert on each other in a given model that is fitted to the data, such as a structural equation model (Friston et al., 1993a; McIntosh and Gonzalez-Lima, 1994). In these settings, a region is a large patch ($\lesssim 1\text{cm}^2$) of cortical tissue that is assumed to synchronize its activity through local cytoarchitecture. This definition strongly relates to that of Hebbian neural assemblies (Hebb, 1949), and is moreover thought to be a relevant spatial scale to study such neural assemblies (Varela et al., 2001). Measures of functional and effective connectivity then characterize the level of interregional integration for each possible pair of regions in a given set of brain regions that has been selected by the investigator. Using functional connectivity as a measure of integration relates a network of N regions to $N(N-1)/2$ functional connections. This potentially large number of connections make results tedious to obtain, present and interpret. For instance, $N = 10$ in Toni et al. (2002), corresponding to $N(N-1)/2 = 45$ functional connections. Direct handling of the connectivity matrix can even become intractable: in Salvador et al. (2005), $N = 96$ and $N(N-1)/2 = 4560$, while $N \gg 100$ in Bellec et al. (2006), making use of data mining techniques such as multidimensional scaling or hierarchical clustering mandatory.

An alternative to further reduce the complexity of connectivity studies is to resort to a measure called integration and denoted by I. Integration, as defined by Tononi et al. (1994), derives from an information theoretical measure called mutual information (Cover and Thomas, 1991), Kullback–Leibler information proper (Whittaker, 1990), or multiinformation function (Studený and Vejnarová, 1998). Its objective is to capture the global level of statistical dependence within a brain network. It has been applied to fMRI to capture the eponymous feature of functional brain integration (Sporns et al., 2000) through the so-called functional cluster index (Tononi et al., 1998b; Foucher et al., 2005). Measures derived from I have mostly been applied as a way to describe and characterize very complex models of structural connectivity and summarize their informational content, which could not have been apprehended otherwise. Yet, considering a measure of overall connectivity may appear somehow extreme and too coarse, thereby evening out some finer relevant information.

In this paper, we propose to characterize interactions between systems, i.e., sets of regions that can be gathered on anatomical, structural, and/or functional grounds. Since systems represent an intermediate scale between regions and the whole brain, measuring interactions at this level provides an intermediate measure between functional connectivity as measured by correlation and global measures such as integration. To this aim, we show that the measure introduced by Tononi et al. (1994) can be decomposed in a way that reflects within- and between-system integration, similarly to what can be done with inertia and Huygens' formula. With this approach, the number of measures obtained only depends on the number S of systems selected; it is equal to S measures of within-system integration, plus one measure of between-system integration.

The investigation of patients with low-grade glioma (LGG) is an example of application where such approach is of special interest. It is currently well known that slow-growing cerebral lesions such as LGG may induce brain plasticity (Duffau, 2005). This was suggested pre-operatively, due to the fact that patients usually have no or mild deficit despite the frequent invasion of eloquent structures. Moreover, numerous neurofunctional imaging studies have demonstrated that LGG could induce progressive functional reshaping of brain networks, with recruitment of perilesional (Wunderlich et al., 1998; Thiel et al., 2001) and/or contralateral compensatory areas (Fandino et al., 1999; Holodny et al., 2002; Krainik et al., 2004). Intraoperative acute remapping was also observed using direct electrical stimulations, regularly performed all along the surgical resection of LGG (Duffau, 2001). Finally, postoperative fMRI was performed, in particular after removal of LGG in the supplementary motor area (SMA), which had induced a transient postsurgical syndrome: in comparison to the pre-operative state, fMRI showed activations within the SMA and premotor cortex contralateral to the lesion (Krainik et al., 2004). Interestingly, a better knowledge of this plastic potential has enabled to improve functional and oncological results in the surgery of LGG within eloquent areas (Duffau et al., 2003).

Emerging from the literature is thus the hypothesis that a lesioned hemisphere will preferentially recruit its healthy counterpart in order to compensate for the disorganization induced by the tumor and its resection and still be able to process hand movement. This issue has a natural translation in terms of hemispheres as systems: Does interhemispheric (i.e., between-system) integration increase

in patients with a tumor compared to healthy subjects? This seemingly simple hypothesis could not be directly tested until now in neuroimaging for a lack of adequate tool. Introduction of system integration provides a straightforward, yet powerful, framework to assess the validity of this fundamental assumption.

The outline of this paper is the following. In the next section, we present the general background for integration and derive the relationship between total, intra-system, and inter-system integration. The following section is then devoted to demonstrate the relevance of hierarchical integration through the analysis of fMRI data following motor recovery of patients with low-grade glioma located within the SMA. Further issues are addressed in the discussion.

2. Hierarchical integration

2.1. Regions, systems, and the brain

The purpose of this paper is to investigate functional integration occurring within a set of N regions. We now describe our notation regarding regions, systems, and associated time series, as well as our modeling hypotheses. We first assume that the N-dimensional fMRI BOLD time series z_t, $t = 1, \ldots, T$ associated with the N regions are temporally independent and identically distributed (i.i.d.) realizations of a N-dimensional random variable $\boldsymbol{y}$, each region hence being associated with a variable y_n, $n = 1, \ldots, N$. $\boldsymbol{y} = (y_1, \ldots, y_N)$ then stands for the joint variable and is associated to a probability distribution $\mathrm{p}(\boldsymbol{y})$.

Setting $\mathscr{S} = \{1, \ldots, N\}$, we furthermore assume that these N regions are gathered into K subsets, $\mathscr{S} = \{\mathscr{S}_1, \ldots, \mathscr{S}_K\}$. To avoid confusion with regions, each of these sets, $\mathscr{S}_k$, will be called a "system". The corresponding variables are denoted by $\boldsymbol{y}_{\mathscr{S}_k} = (y_n)_{n \in \mathscr{S}_k}$. Note that, with such notation, $\boldsymbol{y}_{\mathscr{S}}$ is equal to $\boldsymbol{y}$.

For instance, when dealing with the investigation of motor recovery for patients with low-grade glioma located within the SMA, the following cortical regions ($N = 6$) have a clear implication in the plasticity process (Krainik et al., 2001, 2004): the two supplementary motor areas, ISMA and CSMA (I standing for "ipsilesional", C for "contralesional"), the two primary sensorimotor cortices, ISMC and CSMC, and the two lateral premotor cortices, IPMC and CPMC. $\mathscr{S}$ is then equal to

$$\mathscr{S} = \{\mathrm{ISMA}, \mathrm{ISMC}, \mathrm{IPMC}, \mathrm{CSMA}, \mathrm{CSMC}, \mathrm{CPMC}\}.$$

To test the hypothesis that regions contralateral to the tumor are more integrated with regions ipsilateral to the tumor after resection of the tumor than before, we could further gather these regions into $K = 2$ systems, comprising all regions within the ipsi- and contralesional hemisphere, respectively, i.e., $\mathscr{S} = \{\mathscr{S}_{\mathrm{IH}}, \mathscr{S}_{\mathrm{CH}}\}$, with

$$\mathscr{S}_{\mathrm{IH}} = \{\mathrm{ISMA}, \mathrm{ISMC}, \mathrm{IPMC}\}$$

and

$$\mathscr{S}_{\mathrm{CH}} = \{\mathrm{CSMA}, \mathrm{CSMC}, \mathrm{CPMC}\}.$$

In this example, a system would hence be a hemisphere, and we would have $\boldsymbol{y}_{\mathrm{IH}} = (y_n)_{n=1,2,3}$ and $\boldsymbol{y}_{\mathrm{CH}} = (y_n)_{n=4,5,6}$. For healthy subjects, we could rather consider that regions are labeled and partitioned according to their laterality. The same regions would hence define the following sets

$$\mathscr{S} = \{\mathrm{LSMA},\ \mathrm{LSMC},\ \mathrm{LPMC},\ \mathrm{RSMA},\ \mathrm{RSMC},\ \mathrm{RPMC}\},$$

where L stands for "left" and R for "right", as well as

$$\mathscr{S}_{\mathrm{LH}} = \{\mathrm{LSMA},\ \mathrm{LSMC},\ \mathrm{LPMC}\}$$

and

$$\mathscr{S}_{\mathrm{RH}} = \{\mathrm{RSMA},\ \mathrm{RSMC},\ \mathrm{RPMC}\}.$$

2.2. Entropy, mutual information, and integration

We now introduce information theoretic concepts, namely entropy and mutual information, and their application to measure functional integration. The entropy of $\mathrm{p}(\boldsymbol{y})$ is given by (Shannon, 1948)

$$H[\mathrm{p}(\boldsymbol{y})] = -\int \mathrm{p}(\boldsymbol{y}) \ln \mathrm{p}(\boldsymbol{y}) \mathrm{d}\boldsymbol{y}. \tag{1}$$

For any two distributions $\mathrm{p}_1(\boldsymbol{y})$ and $\mathrm{p}_2(\boldsymbol{y})$, the Kullback–Leibler information divergence between $\mathrm{p}_1(\boldsymbol{y})$ and $\mathrm{p}_2(\boldsymbol{y})$ is given by (Kullback, 1968)

$$D_{KL}[\mathrm{p}_1(\boldsymbol{y}); \mathrm{p}_2(\boldsymbol{y})] = \int \mathrm{p}_1(\boldsymbol{y}) \ln \frac{\mathrm{p}_1(\boldsymbol{y})}{\mathrm{p}_2(\boldsymbol{y})} \mathrm{d}\boldsymbol{y}.$$

This quantity is always positive, and is equal to zero if and only if $\mathrm{p}_1(\boldsymbol{y})$ and $\mathrm{p}_2(\boldsymbol{y})$ are almost surely equal. Last, for any partition $(\boldsymbol{y}_1, \ldots, \boldsymbol{y}_K)$ of $\boldsymbol{y}$, mutual information (Cover and Thomas, 1991), Kullback–Leibler information proper (Whittaker, 1990), or multiinformation function (Studený and Vejnarová, 1998) is defined as the Kullback–Leibler information divergence between the joint distribution $\mathrm{p}(\boldsymbol{y}_1, \ldots, \boldsymbol{y}_K)$ and the product of the marginal distributions $\prod_{k=1}^{K} \mathrm{p}(\boldsymbol{y}_k)$, i.e.,

$$I[\boldsymbol{y}_1, \ldots, \boldsymbol{y}_K] = D_{KL}\left[\mathrm{p}(\boldsymbol{y}_1, \ldots, \boldsymbol{y}_K); \prod_{k=1}^{K} \mathrm{p}(\boldsymbol{y}_k)\right]. \tag{2}$$

It can also be shown that (see Appendix A or Cover and Thomas, 1991)

$$I[\boldsymbol{y}_1, \ldots, \boldsymbol{y}_K] = \left[\sum_{k=1}^{K} H[\mathrm{p}(\boldsymbol{y}_k)]\right] - H[\mathrm{p}(\boldsymbol{y}_1, \ldots, \boldsymbol{y}_K)]. \tag{3}$$

A major property of mutual information states that this quantity is equal to zero if and only if the compound variables are mutually independent, i.e.,

$$\mathrm{p}(\boldsymbol{y}_1, \ldots, \boldsymbol{y}_K) = \prod_{k=1}^{K} \mathrm{p}(\boldsymbol{y}_k).$$

When different from zero, I measures the amount of global dependence between variables. This quantitative interpretation of mutual information is supported by its interpretation in information theoretic data compression and coding theory (MacKay, 2003). Mutual information, or

integration, was applied to one-dimensional variables, i.e., each variable representing a region, in Tononi et al. (1994). But mutual information can be applied to a much more general setting, i.e., to compound variables, or systems.

2.3. Relation between integration at various levels

Integration is a key quantity to investigate interactions within the brain, for it allows not only to calculate the total functional integration of a brain network, but also to precisely track the origin of this integration and pinpoint the respective contributions of within- and between-system integrations. Indeed, on the one hand we have, at the global, network level, the total integration:

$$I[y_1,\ldots,y_N] = \left[\sum_{n=1}^{N} H[\mathrm{p}(y_n)]\right] - H[\mathrm{p}(y_1,\ldots,y_N)]. \tag{4}$$

On the other hand, we have, at the system level, either the between-system integration

$$I[\boldsymbol{y}_{\mathscr{S}_1},\ldots,\boldsymbol{y}_{\mathscr{S}_K}] = \left[\sum_{k=1}^{K} H[\mathrm{p}(\boldsymbol{y}_{\mathscr{S}_k})]\right] - H[\mathrm{p}(\boldsymbol{y}_{\mathscr{S}_1},\ldots,\boldsymbol{y}_{\mathscr{S}_K})], \tag{5}$$

or the within-system integration of system $\mathscr{S}_k$, that reads

$$I[(y_n)_{n\in\mathscr{S}_k}] = \left[\sum_{n\in\mathscr{S}_k} H[\,\mathrm{p}(y_n)]\right] - H[\mathrm{p}(\boldsymbol{y}_{\mathscr{S}_k})] \tag{6}$$

for all k. Summing Eq. (5) and Eq. (6), for all k, leads to

$$\begin{aligned} &I[\boldsymbol{y}_{\mathscr{S}_1},\ldots,\boldsymbol{y}_{\mathscr{S}_K}] + \sum_{k=1}^{K} I[(y_n)_{n\in\mathscr{S}_k}] \\ &= \left[\sum_{k=1}^{K} H[\mathrm{p}(\boldsymbol{y}_{\mathscr{S}_k})]\right] - H[\mathrm{p}(\boldsymbol{y}_{\mathscr{S}_1},\ldots,\boldsymbol{y}_{\mathscr{S}_K})] \\ &\quad + \sum_{k=1}^{K}\left(\sum_{n\in\mathscr{S}_k} H[\,\mathrm{p}(y_n)] - H[\mathrm{p}(\boldsymbol{y}_{\mathscr{S}_k})]\right). \end{aligned}$$

The terms $H[\mathrm{p}(\boldsymbol{y}_{\mathscr{S}_k})]$ canceling out, simplification of the right-hand side of this equation leads to

$$\left[\sum_{n=1}^{N} H[\,\mathrm{p}(y_n)]\right] - H[\mathrm{p}(\boldsymbol{y}_{\mathscr{S}_1},\ldots,\boldsymbol{y}_{\mathscr{S}_K})].$$

Since $\mathrm{p}(\boldsymbol{y}_{\mathscr{S}_1},\ldots,\boldsymbol{y}_{\mathscr{S}_K})$ is equal to $\mathrm{p}(y_1,\ldots,y_N)$, the right-hand side of the equation is nothing more than $I[y_1,\ldots,y_N]$ of Eq. (4). We have hence proved that

$$I[y_1,\ldots,y_N] = I[\boldsymbol{y}_{\mathscr{S}_1},\ldots,\boldsymbol{y}_{\mathscr{S}_K}] + \sum_{k=1}^{K} I[(y_n)_{n\in\mathscr{S}_k}]. \tag{7}$$

In words, the total integration $I_\mathrm{t} = I[y_1,\ldots,y_N]$ can be decomposed as the sum of a between-system integration term

$$I_\mathrm{bs} = I[\boldsymbol{y}_{\mathscr{S}_1}\ldots,\boldsymbol{y}_{\mathscr{S}_K}]$$

and the sum of each system's integration relative to its regions,

$$I_{\mathrm{ws},k} = I[\boldsymbol{y}_{\mathscr{S}_k}] = I[(y_n)_{n\in\mathscr{S}_k}],$$

or I_k for simplicity:

$$I_\mathrm{t} = I_\mathrm{bs} + \sum_{k=1}^{K} I_k. \tag{8}$$

2.4. Gaussian variables

Gaussianity is a common assumption in fMRI data analysis. Deriving a simple expression for the quantities dealt with earlier in a Gaussian framework is hence highly relevant. Assume that $\boldsymbol{y}$ is Gaussian distributed with mean $\boldsymbol{\mu} = (\mu_n)$ and covariance matrix $\boldsymbol{\Sigma} = (\Sigma_{n,n})$. The joint entropy of $\boldsymbol{y}$ is equal to (Cover and Thomas, 1991)

$$H[\mathrm{p}(\boldsymbol{y})] = \frac{1}{2}\ln[(2\pi e)^N|\boldsymbol{\Sigma}|],$$

where $|\cdot|$ stands for the determinant. The quantity $|\boldsymbol{\Sigma}|$ that appears in this expression is also called the generalized variance (Anderson, 1958). The entropy of each system $\mathscr{S}_k$ is equal to

$$H[\mathrm{p}(\boldsymbol{y}_{\mathscr{S}_k})] = \frac{1}{2}\ln[(2\pi e)^{N_k}|\boldsymbol{\Sigma}_{\mathscr{S}_k,\mathscr{S}_k}|],$$

where N_k is the number of regions comprising system $\mathscr{S}_k$ and $\boldsymbol{\Sigma}_{\mathscr{S}_k,\mathscr{S}_k} = (\Sigma_{l,m})_{l,m\in\mathscr{S}_k}$ the covariance submatrix associated with $\boldsymbol{y}_{\mathscr{S}_k}$. Finally, the entropy of each region is equal to

$$H[\mathrm{p}(y_n)] = \frac{1}{2}\ln[(2\pi e)\Sigma_{n,n}].$$

According to Eq. (4), the total integration is then given by

$$I[y_1,\ldots,y_N] = \frac{1}{2}\ln\left[\frac{\prod_{n=1}^{N}\Sigma_{n,n}}{|\boldsymbol{\Sigma}|}\right]. \tag{9}$$

Note that, if one decomposes the covariance matrix into

$$\boldsymbol{\Sigma} = [\mathrm{diag}(\boldsymbol{\Sigma})]^{1/2}\boldsymbol{R}[\mathrm{diag}(\boldsymbol{\Sigma})]^{1/2},$$

where $\boldsymbol{R}$ is the correlation matrix and $\mathrm{diag}(\boldsymbol{\Sigma})$ is the diagonal matrix of variances, then, using the simple property of determinants $\det(\boldsymbol{AB}) = \det(\boldsymbol{A})\det(\boldsymbol{B})$, one obtains

$$I[y_1,\ldots,y_N] = -\frac{1}{2}\ln|\boldsymbol{R}|.$$

$|\boldsymbol{R}|$ is again analogous to a generalized variance. $I[y_1,\ldots,y_N]$ can be considered as the generalization of a correlation coefficient to a multidimensional system. It is the theoretical counterpart of the minimum discrimination information statistic for the test of independence (Kullback, 1968, Eq. (3.18), p. 303).

The between-system integration can be obtained from Eq. (5) as being

$$I[(\boldsymbol{y}_{\mathscr{S}_k})_{k=1,\ldots,K}] = \frac{1}{2}\ln\left[\frac{\prod_{k=1}^{K}|\boldsymbol{\Sigma}_{\mathscr{S}_k,\mathscr{S}_k}|}{|\boldsymbol{\Sigma}|}\right]. \tag{10}$$

Writing this expression in the form $-\frac{1}{2}\ln(1-R^2)$ shows that $I[(\boldsymbol{y}_{\mathscr{S}_k})_{k=1,\ldots,K}]$ can be considered as a generalization of the multiple correlation coefficient R^2 (Anderson, 1958, Eq. (20), p. 32). It can also be interpreted as the theoretical counterpart of either the log-likelihood ratio criterion (Anderson, 1958, Eq. (16), p. 232) or the minimum discrimination information statistic (Kullback, 1968, Eq. (3.30), p. 305) for testing independent sets of variates. As to within-system integration, it can be derived from Eq. (6) and yields

$$I[(y_n)_{n\in\mathscr{S}_k}] = \frac{1}{2}\ln\left[\frac{\prod_{n\in\mathscr{S}_k}\Sigma_{n,n}}{|\boldsymbol{\Sigma}_{\mathscr{S}_k,\mathscr{S}_k}|}\right] \tag{11}$$

for all k. Based on these results, it is incidentally straightforward to check that Eq. (7) holds for Gaussian variables (see Appendix B).

2.5. Inference

Given the model parameters $\boldsymbol{\mu}$ and $\boldsymbol{\Sigma}$, all quantities of interest can be uniquely determined by Eqs. (9)–(11). Unfortunately, since the true values of $\boldsymbol{\mu}$ and $\boldsymbol{\Sigma}$ are unknown and only partly accessible through the data, so are the values of integration, which must hence be inferred from the data. To this aim, we resort to a Bayesian numerical sampling scheme that approximates the posterior distribution of the parameters of interest in a group analysis (see Appendix C, or Marrelec et al., 2006b). From there, all statistics can easily be obtained. For instance, any integration I can be approximated from L samples $(I^{[l]})$ originating from $\mathrm{p}(I|\boldsymbol{y})$ by

$$I \approx M \pm \sqrt{V}$$

with

$$M = \frac{1}{L}\sum_{l=1}^{L} I^{[l]}$$

and

$$V = \frac{1}{L}\sum_{l=1}^{L}(I^{[l]} - M)^2.$$

More generally, this method provides a simple way to approximate the posterior probability $\mathrm{P}(A|\boldsymbol{y})$ of any (simple or compound) assertion A related to the within-system, the between-system, and the total integration measures introduced here. For instance, the posterior probability that a total integration $I_{t,1}$ is simultaneously lower than two other total integrations $I_{t,2}$ and $I_{t,3}$, i.e., $A =$ "$(I_{t,1} < I_{t,2})$ and $(I_{t,1} < I_{t,3})$", can be approximated by

$$\mathrm{P}(A|\boldsymbol{y}) \approx \frac{1}{L}\#\left\{l : I_{t,1}^{[l]} < I_{t,2}^{[l]} \text{ and } I_{t,1}^{[l]} < I_{t,3}^{[l]}\right\},$$

where # stands for the cardinal function of a set. Such a procedure nicely eliminates the issue usually caused by multiple comparisons and the subsequent need to devise ad hocqueries in classical statistics, since multiple comparisons are taken into account in the comparison. This is not a specific feature of our approach, but is characteristic of the Bayesian paradigm.

A convenient index of the validity of A is then provided by the so-called evidence for A given $\boldsymbol{y}$, defined as (Jaynes, 2003, Section 4.2)

$$e(A|\boldsymbol{y}) = 10\log_{10}O(A|\boldsymbol{y}),$$

where $O(A|\boldsymbol{y})$ is the posterior odd ratio of A, defined as

$$O(A|\boldsymbol{y}) = \frac{\mathrm{P}(\mathrm{A}|\boldsymbol{y})}{\mathrm{P}(\neg\mathrm{A}|\boldsymbol{y})} = \frac{\mathrm{P}(\mathrm{A}|\boldsymbol{y})}{1-\mathrm{P}(\mathrm{A}|\boldsymbol{y})},$$

where $\neg A$ stands for the negation of A. Evidence is measured in decibels (dB) (see Table 1).

3. Real data

3.1. Imaging and preprocessing

The MR protocol was carried out with a General Electric 1.5T Signa system. Functional MRI using BOLD contrast was performed. The protocol included: (1) two runs comprising 42 T_2^*-weighted functional volumes each, each volume covering the whole frontal lobes (TR/TE/flip angle: 3000 ms/60 ms/90°, 20 contiguous slices per volume, 5 mm slice thickness, in-plane pixel size: 3.75 mm × 3.75 mm) and (2) one axial inversion recovery three-dimensional T_1-weighted image for anatomical localization.

Six right-handed patients with low-grade glioma close to the supplementary motor area were scanned both upon admission and after removal of the glioma and recovery of the motor abilities. The tumor was located in the right hemisphere for three patients, in the left hemisphere for the three others. The experimental design protocol consisted of two different blocked-trial tasks: self-paced flexion/extension of the fingers of the right or left hand, depending on the session. Before the experiment started, all subjects practiced each movement to keep frequency, amplitude, acceleration, and strength constant. The subjects were asked to perform the tasks at a movement rate of 0.5 Hz. The paradigm was block-designed, alternating rest (R) and activation (A), and consisted of seven epochs of 18 s each for either activation or rest (total duration of each run: 2 min 06 s in this order: R–A–R–A–R–A–R). The task instructions were auditory-cued using a digital audio tape and presented using standard headphones

Table 1
Evidence, odds, and probability (from Jaynes, 2003, Table 4.1, p. 93)

e (dB)	O	P
0	1:1	1/2
3	2:1	2/3
6	4:1	4/5
10	10:1	10/11
20	100:1	100/101
30	1000:1	0.999
40	10^4:1	0.9999
$-e$ (dB)	$1/O$	$1-P$

customized for fMRI experiments and inserted in a noise-protecting helmet that provided isolation from scanner noise. Direct observation of the tasks was performed by an investigator during the fMRI acquisitions. Seven healthy right-handed male volunteers were also scanned after giving informed consent set by the local ethic committee.

Preprocessing was performed in MATLAB®[1] with the SPM99 software.[2] The first six images of each run were discarded for signal stabilization. For each subject, images were corrected for rigid subject motion with the first volume of each run used as a reference, and transformed stereotactically to common spatial coordinates using the standard template of the Montreal Neurologic Institute (MNI). The resulting images were smoothed with a Gaussian isotropic spatial filter (FWHM $= 5 \times 5 \times 5$ mm).

3.2. Region and signal selection

According to previous studies (Krainik et al., 2001, 2004), six cortical regions were selected: ISMA, ISMC, IPMC, CSMA, CSMC, and CPMC. These regions were manually drawn by an expert onto normalized T_1-weighted anatomical images without reference to the activation patterns, using a standard sulcal atlas (Talairach and Tournoux, 1988; Naidich et al., 2001). Coregistration across anatomical and functional images and across subjects was assessed on anatomical landmarks located in the vicinity of the regions of interest (ROIs) such as the interhemispheric fissure, the "hand knob", and the crossing between precentral and frontal superior sulci. We also used standardized ROIs to avoid an effect of ROIs volume across subjects.

The signal characteristic of each region was then selected as the spatial average of the time course of all voxels within the region. This signal was then translated and scaled to be of zero mean and unit variance. We finally obtained 6 (patients) $\times$ 2 (ipsi- and contralateral hand movements) $\times$ 2 (before and after surgery) time courses of 36 times samples for patients, and 7 (subjects) $\times$ 2 (left- and right-hand movements) for the control group.

3.3. Hierarchical integration

In the case of a patient's cortical motor network, the total integration yields

$$I_t = \frac{1}{2} \ln \left[\frac{\prod_{n=1}^{6} \Sigma_{n,n}}{|\mathbf{\Sigma}|} \right], \tag{12}$$

and the interhemispheric (i.e., between-system) integration reads

$$I_i = \frac{1}{2} \ln \left[\frac{|\mathbf{\Sigma}_{IH,IH}| \cdot |\mathbf{\Sigma}_{CH,CH}|}{|\mathbf{\Sigma}|} \right]. \tag{13}$$

[1] The Mathworks Inc., Natick, MA, USA.

[2] Wellcome Department of Cognitive Neurology, UCL, London, UK.

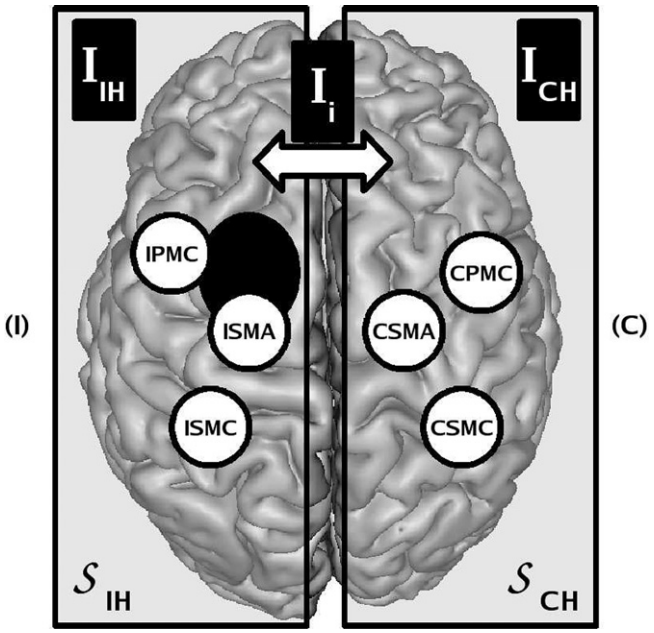

Fig. 1. Real data. Partitioning of the six regions into two systems: ipsi- and contralesional hemispheres.

As to both intrahemispheric (i.e., within-system) integrations, they read

$$I_{IH} = \frac{1}{2} \ln \left[\frac{\prod_{n=1,2,3} \Sigma_{n,n}}{|\mathbf{\Sigma}_{IH,IH}|} \right] \quad \text{and} \quad I_{CH} = \frac{1}{2} \ln \left[\frac{\prod_{n=4,5,6} \Sigma_{n,n}}{|\mathbf{\Sigma}_{CH,CH}|} \right], \tag{14}$$

respectively. In this setting, Eq. (8) states that the total integration I_t can be decomposed as the sum of an interhemispheric integration term I_i and the intrahemispheric integration terms of each hemisphere relative to their regions, I_{IH} and I_{CH}:

$$I_t = I_i + I_{IH} + I_{CH}. \tag{15}$$

The regions, systems, and corresponding integrations are schematized in Fig. 1. For healthy subjects, the same results hold with "RH" and "LH" instead of "IH" and "CH".

We approximated the posterior distributions for all integration measures according to the sampling scheme detailed earlier and Eqs. (12)–(14). The samples so obtained were then used to calculate the corresponding means and standard errors, as well as to test for differences.

3.4. Results

The estimated integration measures are summarized in Fig. 2. We also compared the integration measures of control and patient groups. In the remainder, a difference is declared to be significant[3] when the corresponding evidence

[3] Since inference is performed in a Bayesian framework, the terms "significant" and "significance" are not used in their usual, frequentist sense (i.e., when comparing the p-value of a null hypothesis to a given threshold) but in the sense of "above threshold".

is larger than a threshold of 10 dB. The interested reader may refer to a comprehensive report of the evidences of all pairwise comparisons in Table 2 (top – for total integration, bottom – for interhemispheric integration) and Table 3 (for intrahemispheric integration). In the following, we only mention results that are relevant to our hypotheses. Evidences are denoted e throughout the text. When some observed feature was the joint result of several simple evidences, it was denoted e_{compound}. For instance, to prove that the total integration is significantly lower for patients performing an ipsilesional hand movement post-operatively than for patients performing the same movement pre-operatively, one has to compute the evidence of the assertion

$$A_{\text{I}} = \text{“}I_{\text{t,Po/I}} < I_{\text{t,Pr/I}}\text{”};$$

similarly, to prove that the total integration is significantly lower for patients performing a contralesional hand movement post-operatively than for patients performing the same movement pre-operatively, one has to compute the evidence of the assertion

$$A_{\text{C}} = \text{“}\mathrm{I}_{\text{t,Po/C}} < I_{\text{t,Pr/C}}\text{”}.$$

Now, if one wants to prove that the total integration is significantly lower for patients post-operatively than for patients pre-operatively (regardless of the movement), one must compute the evidence of the assertion

$$A = \text{“}A_{\text{I}} \quad \text{and} \quad A_{\text{C}}\text{”}.$$

Assertion A is a compound assertion and, as such, its corresponding evidence is denoted e_{compound}. For a non-significant compound assertion, we reported the highest marginal evidence.

For the control group, there was globally no significant difference in either the total (I_{t}) or interhemispheric (I_{i}) integration when comparing a left- and a right-hand movement ($|e| = 2.0$ dB in both cases). Also, for a given hand movement, there existed a significant dominance of the intrahemispheric integration of the hemisphere contralateral to the hand movement ($e_{\text{compound}} = 10.5$ dB), i.e., of the left hemisphere over the right one for a right-hand movement ($e = 17.9$ dB) and of the right hemisphere over the left one for a left-hand movement ($e = 11.5$ dB). Globally, the laterality of movement had little influence on the integration, for the level of intrahemispheric integration in the hemisphere ispilateral (resp. contralateral) to the hand movement did not significantly depend on the hand used. Ipsilaterally to the hand movement, I_{LH} for a left-hand movement was not different from I_{RH} for a right-hand movement ($|e| = 0.4$ dB); contralaterally to the hand movement, I_{RH} for a left-hand movement was not significantly different from I_{LH} for a right-hand movement ($|e| = 3.3$ dB). In other words, the motor network behaved

Table 2
Real data

	H/R	H/L	Pr/I	Pr/C	Po/I
Total integration					
H/L	−2.0				
Pr/I	1.8	3.5			
Pr/C	9.6	**12.4**	6.9		
Po/I	**−20.9**	**−19.2**	**−21.5**	**<−30.0**	
Po/C	**−25.2**	**−19.5**	**−25.2**	**<−30.0**	0.1
Interhemispheric integration					
H/L	−2.0				
Pr/I	−2.5	0.52			
Pr/C	**24.0**	**25.2**	**21.5**		
Po/I	**−15.9**	**−14.0**	**−12.6**	**<−30.0**	
Po/C	3.9	5.7	5.6	**−13.6**	**25.2**

Changes in total (top) and interhemispheric (bottom) integration as measured by evidence (in dB, see Section 2.5). Significant differences (absolute values higher than 10 dB) are emphasized in bold. Positive values correspond to increases, negative values to decreases. H: healthy subjects; R: right hand; L: left hand; Pr: patients pre-operatively; Po: patients post-operatively; I: ipsilesional hand; C: contralesional hand. For instance, the total integration is significantly higher for Pr/C than for H/L, with an evidence $e(I_{\text{Pr/C}} > I_{\text{H/L}}|\boldsymbol{y}) \approx 12.4$ dB.

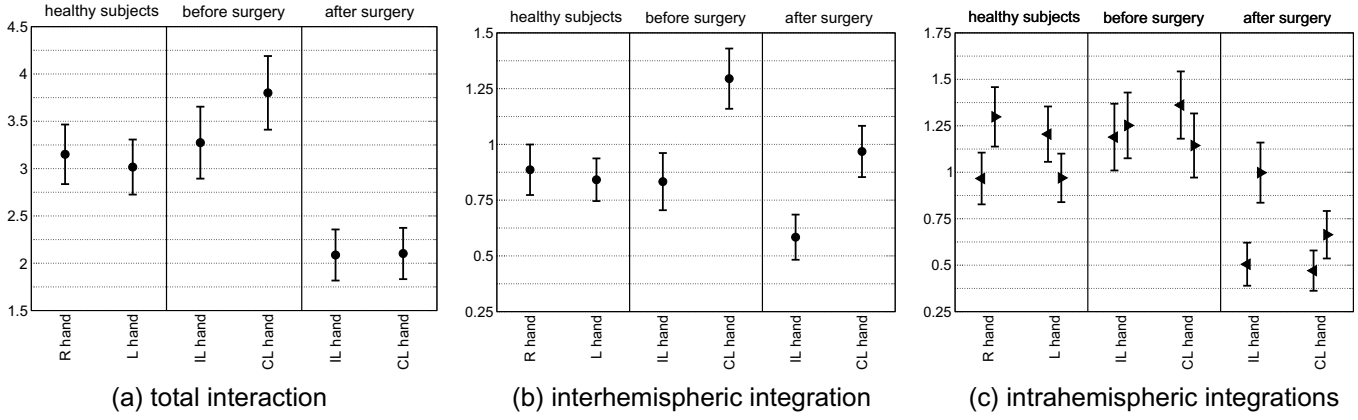

Fig. 2. Real data. Total integration I_{t} (left), interhemispheric integration, I_{bs} (middle), and intrahemispheric integration (right) for healthy subjects and patients before surgery, and after surgery and recovery of the motor ability. For healthy subjects, intrahemispheric integration of the left (resp. right) hemisphere is represented with a right (resp. left) pointing arrow. For patients, intrahemispheric integration of the lesioned (resp. healthy) hemisphere is represented with a left (resp. right) pointing arrow.

Table 3
Real data

	H/R/R	H/R/L	H/L/R	H/L/L	Pr/I/I	Pr/I/C	Pr/C/I	Pr/C/C	Po/I/I	Po/I/C	Po/C/I
H/R/L	**17.9**										
H/L/R	9.2	−3.3									
H/L/L	0.4	**−13.6**	**−11.5**								
Pr/I/I	7.1	−3.3	−0.2	6.9							
Pr/I/C	9.5	−1.4	1.5	9.5	2.6						
Pr/C/I	**13.2**	2.0	−4.5	**13.8**	4.4	3.0					
Pr/C/C	5.2	−4.5	−2.0	5.6	−1.1	−2.7	−9.9				
Po/I/I	**−22.2**	**<−30.0**	**<−30.0**	**−25.2**	**<−30.0**	**<−30.0**	**<−30.0**	**<−30.0**			
Po/I/C	1.0	−9.6	−7.0	0.7	−6.1	−7.8	**−11.7**	−4.3	**27.0**		
Po/C/I	**−25.2**	**<−30.0**	**−30**	**−24.0**	**<−30.0**	**<−30.0**	**<−30.0**	**<−30.0**	−2.0	**−24.0**	
Po/C/C	**−12.3**	**<−30.0**	**−23.0**	**−12.7**	**−20.9**	**−24.0**	**<−30.0**	**−19.2**	7.16	**−13.1**	**12.4**

Changes in intrahemispheric integration as measured by evidence (in dB, see Section 2.5). Significant differences (absolute values higher than 10 dB) are emphasized in bold. Positive values correspond to increases, negative values to decreases. The different datasets are classified as follows: subject type/hand movement/hemisphere. H: healthy subjects; Pr: patients pre-operatively; Po: patients post-operatively; R: right; L: left; I: ipsilesional; C: contralesional. For instance, the intrahemispheric integration of Pr/C/I is significantly higher than that of H/L/L, with $e(I_{\mathrm{Pr/C/I}} > I_{\mathrm{H/L/L}}|\boldsymbol{y}) \approx 13.8$ dB.

rather symmetrically relative to simple-hand movements as far as functional integration was concerned: a shift in hand laterality essentially induced a shift in intrahemispheric integration, i.e., decrease ipsilaterally and increase contralaterally to the movement.

For patients before surgery, a pattern similar to that of the control group was observed within the group: no difference in total integration ($|e| = 6.9$ dB), symmetry of intrahemispheric integration relative to movement ($|e| < 3.0$ dB). Unlike the control group, while there could exist a difference between intrahemispheric integrations for an contralesional hand movement ($e = 9.9$ dB, close to significance), no difference was found for a ipsilesional hand movement ($|e| = 2.6$ dB). Comparing the group of patients before surgery during an ipsilesional hand movement to the control group, no difference was found in total integration ($|e| < 3.5$ dB), intrahemispheric integration ($|e| < 7.1$ dB), as well as interhemispheric integration during an ipsilesional hand movement ($|e| < 2.5$ dB). By contrast, interhemispheric integration during contralesional hand movement was significantly stronger ($e_{\mathrm{compound}} = 18.5$ dB) than both during an ipsilesional movement ($e = 21.2$ dB) and what could be observed in the control group ($e > 24.0$ dB).

For patients after surgery and recovery, significant decreases in total ($e_{\mathrm{compound}} = 21.5$ dB) and interhemispheric ($e_{\mathrm{compound}} = 9.9$ dB, close to significance) integrations were found for both hand movements, as well as a significant decrease ($e_{\mathrm{compound}} > 30$ dB) in ipsilesional intrahemispheric integration compared to before surgery and the control group. Similarly to before surgery, interhemispheric integration during contralesional hand movement was significantly stronger than during an ipsilesional movement ($e = 21.2$ dB). Unlike before surgery, contralesional integration after surgery was found to be modulated by hand movement, significantly decreasing from an ipsilesional to a contralesional hand movement ($e = 13.1$ dB).

In summary, we observed the four following major changes ($e_{\mathrm{compound}} = 12.4$ dB):

- the total integrations I_{t} measured for both hand movements were significantly lower ($e_{\mathrm{compound}} = 14.4$ dB) for patients after surgery and recovery than they were for healthy subjects and patients before surgery;
- unlike healthy subjects ($|e| = 2.0$), the interhemispheric integration I_{i} significantly increased ($e_{\mathrm{compound}} = 20.0$ dB) when switching from ipsilesional to contralesional hand movement for patients, both before and after surgery;
- the ipsilesional intrahemispheric integration I_{IH} measured for both hands was significantly lower ($e_{\mathrm{compound}} = 18.2$ dB) for patients after surgery and recovery than it was before surgery and for the control group;
- differing from before surgery ($|e| = 1.1$ dB), a significant difference between the two intrahemispheric integrations I_{IH} and I_{CH} when patients after surgery and recovery performed ipsilateral hand movement ($e = 27.0$ dB).

4. Discussion

In this paper, we showed that the total integration can be decomposed as the sum of within-system integrations and a between-system integration, allowing for a hierarchical approach of integration (e.g., by considering the relative contributions of regions, hemispheres, and the whole network). We expressed all quantities as functions of the covariance matrix in a Gaussian framework and used a Bayesian sampling scheme to perform group inference from data. We applied this method to a dataset that both demonstrated the importance of I as a measure of integration in fMRI data analysis and illustrated the relevance of the method to investigate systems' integration.

From a methodological perspective, the concordance between expected results in patients with LGG and calculations obtained with hierarchical integration pleads for the relevance of this measure in fMRI analysis of functional interactions. Integration has only been used in fMRI in conjunction with the so-called functional cluster index, or

FCI (Tononi et al., 1998b; Foucher et al., 2005), which is defined as the ratio of a subsystem's integration and its interaction with the rest of the system. Also, a degenerate form of integration is commonly used to measure integration, namely correlation ρ. Indeed, when one artificially considers a network of two regions (i.e., with two 1-region systems), where each region also stands as a system, the total integration yields (Kullback, 1968; Marrelec et al., 2005)

$$I_t = -\frac{1}{2}\ln(1-\rho^2)$$

and is equal to the between-system integration, both within-system integration terms being equal to zero. Correlation is a common measure of functional connectivity in fMRI (e.g., Dodel et al., 2005; Achard et al., 2006). Yet its generalization to quantify interactions between compound variables has only led to correlation-based n-to-1 measures (Jiang et al., 2004). In this context, mutual information applied to systems appears as a natural, principled and powerful generalization of correlation. We advocate that it is a valid measure of functional brain integration in fMRI, whose use would prove relevant to investigate integration within systems composed of several regions. The framework proposed in this paper supports the use of systems and hierarchical analyses in investigation of functional brain integration, since it relates brain integration at various levels. Indeed, closer examination of systems can lead to divide them further into subsystems. For example, a network associated to visuomotor tasks can arguably be separated into visual and motor systems; the motor system itself can, in turn, be decomposed into cerebellum, striatum, and cortex, and so forth.

Many cases exist where such a hierarchical approach would prove valuable. Functional MRI data analysis has brought important information relative to the neural correlates of brain processes. However, this knowledge mostly originates from activation maps and, hence, merely provides localization of the network involved. The validity of new findings was reinforced by the possibility of comparing these localizations with previous findings coming from other fields. However, these previous findings display a wide variety of nature (anatomical or functional; if functional, electromagnetic, metabolic, or hemodynamic) and scale (temporal and spatial), making comparisons far from obvious and highly subjective (Horwitz and Poeppel, 2002). Due to its intrinsic complexity, this issue is even more blatant for the study of integration than it is for localization. Hierarchical integration will, we believe, remove one obstacle to the interpretation of fMRI results in the light of results from other fields, such as neuroanatomy, electrophysiology, case studies, and neurosurgery.

For instance, the case examined in this paper—functional plasticity of the cortical motor network induced by slow tumor growth and surgery—is a compelling illustration that hierarchical integration analysis makes it possible, and convenient, to compare the network's interaction features as observed through fMRI data with clinical experience. Indeed, contrahemispheric recruitment is a well-established hypothesis in many tumor and stroke pathologies that could not be tested as such using previous methodological framework. Some works on strokes used laterality indices based on activation maps to quantifiy the degree of contralateral recruitment (Cramer et al., 1997; Calautti and Baron, 2003), but this approach has several drawbacks, such as concentrating on the primary motor cortices, being threshold-dependent, and only taking activation phenomena into account. On the other hand, our approach provides an adapted framework in which such quantification can be efficiently made at the level of an hemisphere. Furthermore, this quantification will not only take activation, but also more generally connectivity effects, into account. The fact that our analysis strongly corroborates the hypothesis of contralesional recruitment is, furthermore, evidence of the relevance of integration in fMRI.

From the analysis of the real data, it was first shown that, pre-operatively, in comparison to the control population of healthy volunteers, there was a significant increase in the interhemispheric integration for a contralesional hand movement. These data fit well with the results of the literature using neurofonctional imaging in cases of brain lesions, especially stroke, which have demonstrated a recruitment of the contralesional homologous (Rijntjes and Weiller, 2002), due to changes in the transcallosal inhibition and interhemispheric competition (Murase et al., 2004). In slow-growing LGG, numerous pre-operative neurofunctional imaging studies not only showed activations within the contralesional hemisphere (Fandino et al., 1999; Holodny et al., 2002; Krainik et al., 2004), but also supported the actual functional role of such recruitment—via the recent use of transcranial magnetic stimulations (Thiel et al., 2005).

Second, post-operatively, a modulation of the interhemispheric integration with the laterality of hand movement was equally found, again in accordance with previous neuroimaging studies performed after functional recovery following a surgical resection of LGG located within the motor network—which showed a contralesional recruitment (Krainik et al., 2004). Moreover, there was a decrease in the intrahemispheric ipsilesional integration—while the intrahemispheric contralesional integration was preserved to a certain extent. This observation is in agreement with the fact that a surgery has been performed within the ipsilesional hemisphere, inducing an "acute" lesion, in opposition to the pre-operatively slow-growing LGG that has little impact on the pre-operative ipsilesional intrahemispheric integration due to an intrahemispheric reorganization (Duffau, 2005). Indeed, it is well known that the tumor resection itself, when performed within eloquent areas, may generate a dysconnection syndrome, in particular in the premotor region, explaining the occurrence of a transient SMA syndrome (Fontaine et al., 2002).

However, the precise mechanisms of such plasticity remain incompletely understood, especially at the level of a whole functional network (i.e., not only regarding one cortical area separately). Furthermore, it is still difficult to predict, before the surgery, the pattern of post-operative remapping—thus the limit of the plastic potential for each patient. It may be hypothesized that integration changes could be related to the characteristics of the lesion of functional areas (tumoral infiltration and surgical resection). As a consequence, it remains necessary to better study the individual connectivity, namely, the relationships between areas involved in a large functional network, and to analyze the dynamics of such interrelations in longitudinal series (particularly before and following surgery). In other words, what are the neural correlates, e.g., in terms of functional integration, of brain plasticity and, more particularly, interhemispheric compensation?

Hierarchical analysis removes the implicit tradeoff that usually had to be kept regarding the number of regions involved in interactivity investigation with, e.g., correlation analysis. Indeed, incorporating many regions has the advantage of producing a more comprehensive network and, hence, analysis. However, it also implies a significant increase in the amount of information that has to be processed by a human operator. Consequently most methods (with exceptions, e.g., Salvador et al., 2005; Bellec et al., 2006) only use a few regions. With hierarchical analysis, it would be possible to use many regions, but only a few systems. Interestingly, the information contained in integration is also contained in the correlation matrix, since the former can be considered as a one-dimensional "summary" of the latter. This can be evidenced by taking a closer look at the estimated correlation matrices corresponding to the various conditions, represented in Fig. 3. According to Eqs. (12)–(14), the integration of a system (respectively, of the whole brain) is a function of the system submatrix (respectively, the full matrix). Simply looking at the correlation matrices for patients in Fig. 3 clearly shows (i) a global decrease in correlations after surgery compared to before surgery and healthy subjects; (ii) a decrease in correlations within the ipsi-lesional hemisphere after surgery compared to before surgery or healthy subjects; and (iii) an increase in correlations between ipsi- and contralesional hemispheres before surgery compared to healthy subjects. We are hence able to visually confirm the results of integration using the correlation matrices. Integration provides an efficient and principled way to quantify this global level of interaction. As illustrated on this example, I appears to be more a systems property rather than associated with a particular region or its connections. In this sense, it seems neutral to the internal organization of that network, e.g., whether ISMA is connected to ISMC.

From a methodological standpoint, several features of our method could be improved regarding the estimation of integration. Since the underlying model assumes i.i.d. data, no particular temporal coherence or structure is granted to the data. For this reason, it fails to grasp any such features of the signal as the influence of the block design or potential temporal autocorrelation. While such

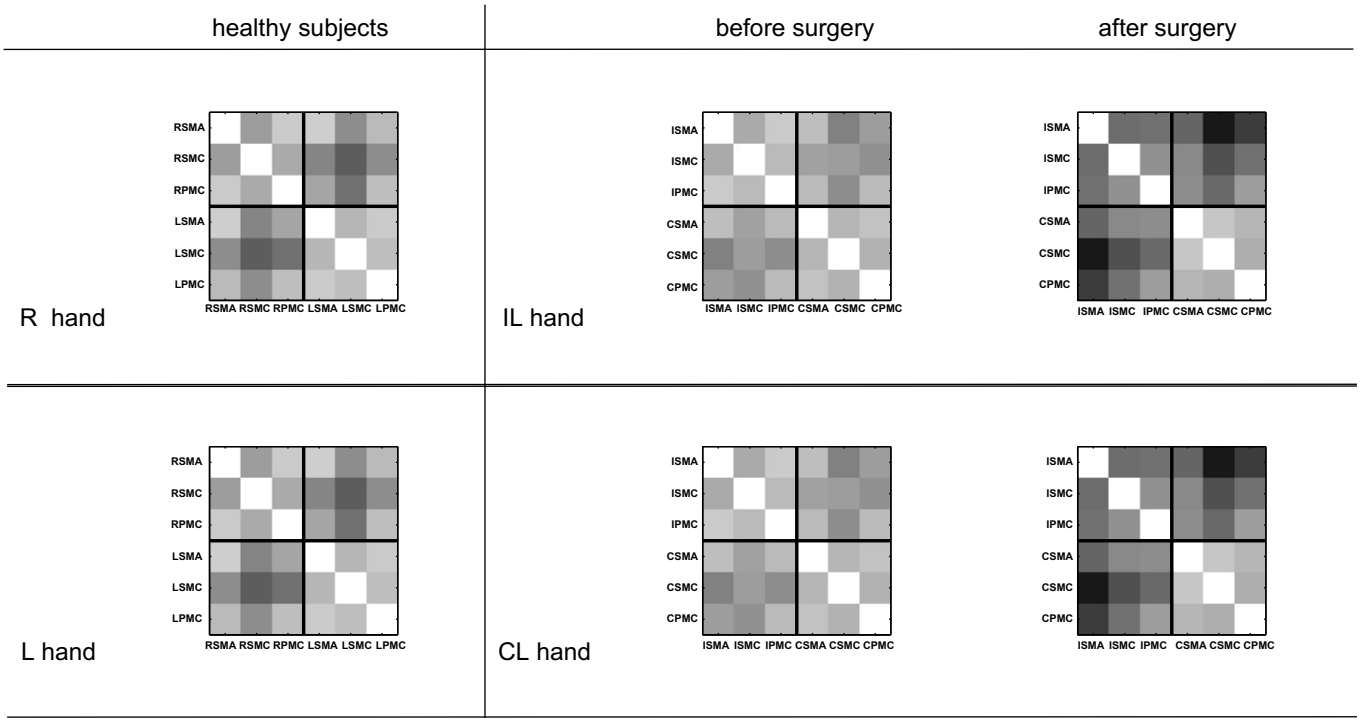

Fig. 3. Real data. Estimated correlation matrix (posterior mean) corresponding to the different conditions (gray scale with black corresponding to 0 and white to 1).

effects are obviously present in the data, normal quantile plots of the time series analyzed in this article showed that deviations from normality are actually rather limited. Globally, we believe that the approach expounded here provides a good, simple, and fast approximation of the results that would be obtained by more refined methods. Even though the model provided is very simple at the individual level, the major part of the variability, which occurs between subjects, is correctly taken into consideration by our model.

A last point that needs to be mentioned is region and signal selection. Many methods exist to define regions pertaining to a network, ranging from anatomical delineation to functional selection based on significant activation or inter-correlation; similarly, the signal corresponding to a given region can be obtained by taking the raw or filtered signal of a voxel, by spatial averaging over a region, by PCA, or ICA (for a review, see, e.g. Marrelec et al., 2006a). Different ways to proceed along this first step may give different results in integration. The influence on hierarchical integration has yet to be assessed. Nonetheless, this issue is omnipresent in the field of functional brain connectivity. While the effects that we investigated in the real data of this paper were induced by tumor growth and surgery—and, hence, expected to be rather large—being able to detect integration variations in healthy subjects might involve more subtle ways to select the regions and corresponding signals.

5. Conclusion and perspectives

The objective of this article was to provide a methodological framework for the hierarchical examination of functional brain integration. To provide an investigation tool that is more refined than global integration, we proposed to apply integration at a system's level. We also showed that a relationship exists between integrations at different levels, allowing for a hierarchical analysis of integration. We illustrated the relevance of this approach by applying it to patients with low-grade glioma, in order to extract information related to the reorganization induced by lesional brain plasticity.

The measures of integration seemed to be in accordance with the data collected during the surgical procedures and with the data provided by neurofunctional imaging (in both the pre- and post-operative stages). Indeed, they were able to detect the effects induced by the slow-growing LGG then by the acute resection. Consequently, this method could be useful concerning (1) clinical applications (selection and planning of brain tumor surgeries) and (2) fundamental issues (study of the mechanisms of brain plasticity).

The proposed approach could also prove useful with a wide range of protocols and networks, when one has to deal with several to many regions of interest but is rather interested in an effect that is not hypothesized to be localized in one particular region but could rather be observed at a large scale. The study of laterality in language or of recovery in stroke patients belongs to such examples.

Appendix A. Mutual information and entropy

The entropy of each $\mathrm{p}(\boldsymbol{y}_k)$ can be expanded as

$$H[\mathrm{p}(\boldsymbol{y}_k)] = -\int \mathrm{p}(\boldsymbol{y}_k)\ln \mathrm{p}(\boldsymbol{y}_k)\mathrm{d}\boldsymbol{y}_k = -\int \mathrm{p}(\boldsymbol{y}_1,\ldots,\boldsymbol{y}_K)\ln \mathrm{p}(\boldsymbol{y}_k)\prod_{k=1}^{K}\mathrm{d}\boldsymbol{y}_k.$$

Hence

$$\sum_{k=1}^{K} H[\mathrm{p}(\boldsymbol{y}_k)] = -\int \mathrm{p}(\boldsymbol{y}_1,\ldots,\boldsymbol{y}_K)\ln[\mathrm{p}(\boldsymbol{y}_1)\cdots\mathrm{p}(\boldsymbol{y}_K)]\prod_{k=1}^{K}\mathrm{d}\boldsymbol{y}_k$$

and

$$\sum_{k=1}^{K} H[\mathrm{p}(\boldsymbol{y}_k)] - H[\mathrm{p}(\boldsymbol{y}_1,\ldots,\boldsymbol{y}_K)] = -\int \mathrm{p}(\boldsymbol{y}_1,\ldots,\boldsymbol{y}_K)\ln\frac{\mathrm{p}(\boldsymbol{y}_1)\cdots\mathrm{p}(\boldsymbol{y}_K)}{\mathrm{p}(\boldsymbol{y}_1,\ldots,\boldsymbol{y}_K)}\prod_{k=1}^{K}\mathrm{d}\boldsymbol{y}_k,$$

which is the mutual information, $I[\boldsymbol{y}_1,\ldots,\boldsymbol{y}_K]$.

Appendix B. Integration for Gaussian variables

We have

$$\begin{aligned}
I[(\boldsymbol{y}_{\mathscr{S}_k})_{k=1,\ldots,K}] + \sum_{k=1}^{K} I[(y_n)_{n\in\mathscr{S}_k}] &= \frac{1}{2}\ln\left[\frac{\prod_{k=1}^{K}|\boldsymbol{\Sigma}_{\mathscr{S}_k,\mathscr{S}_k}|}{|\boldsymbol{\Sigma}|}\right] + \sum_{k=1}^{K}\frac{1}{2}\ln\left[\frac{\prod_{n\in\mathscr{S}_k}\Sigma_{n,n}}{|\boldsymbol{\Sigma}_{\mathscr{S}_k,\mathscr{S}_k}|}\right]\\
&= \frac{1}{2}\ln\left[\frac{\prod_{k=1}^{K}|\boldsymbol{\Sigma}_{\mathscr{S}_k,\mathscr{S}_k}|}{|\boldsymbol{\Sigma}|}\cdot\prod_{k=1}^{K}\frac{\prod_{n\in\mathscr{S}_k}\Sigma_{n,n}}{|\boldsymbol{\Sigma}_{\mathscr{S}_k,\mathscr{S}_k}|}\right]\\
&= \frac{1}{2}\ln\left[\frac{\prod_{k=1}^{K}|\boldsymbol{\Sigma}_{\mathscr{S}_k,\mathscr{S}_k}|}{|\boldsymbol{\Sigma}|}\cdot\frac{\prod_{n=1}^{N}\Sigma_{n,n}}{\prod_{k=1}^{K}|\boldsymbol{\Sigma}_{\mathscr{S}_k,\mathscr{S}_k}|}\right]\\
&= \frac{1}{2}\ln\left[\frac{\prod_{n=1}^{N}\Sigma_{n,n}}{|\boldsymbol{\Sigma}|}\right]\\
&= I[y_1,\ldots,y_N].
\end{aligned}$$

Appendix C. Inference

For our Bayesian analysis, we used the following hierarchical model. For each subject s, $s = 1,\ldots,S$, the BOLD signal measured at time t for the N regions is assumed to be Gaussian distributed with mean $\boldsymbol{\mu}_s$ and covariance matrix $\boldsymbol{\Sigma}_s$. We further assume that all subjects originate from a homogeneous population with characteristic covariance matrix $\boldsymbol{\Sigma}_0$. Specifically, we set the following:

- for each subject s, $s = 1, \ldots, S$:
  - the likelihood of the data given the subject parameters $\boldsymbol{\mu}_s$ and $\boldsymbol{\Sigma}_s$ reads $(\boldsymbol{y}_s|\boldsymbol{\mu}_s, \boldsymbol{\Sigma}_s) \sim \mathcal{N}(\mu_s, \boldsymbol{\Sigma}_s)$;
  - the prior distribution for $\boldsymbol{\mu}_s$ is set to a noninformative uniform prior: $\mathrm{p}(\boldsymbol{\mu}_s) \propto$ constant;
  - we choose a conjugate prior for $\boldsymbol{\Sigma}_s$:

    $(\boldsymbol{\Sigma}_s|\boldsymbol{\Sigma}_0, v_0) \sim \text{Inv-Wishart}_{v_0}(\boldsymbol{\Sigma}_0^{-1})$.

    While the use of a conjugate prior greatly simplifies calculations, the proposed model can still efficiently capture the inter-subject variability through the tuning of parameter v_0.
- the prior for $\boldsymbol{\Sigma}_0$ is set as a noninformative Jeffreys' prior:

  $\mathrm{p}(\boldsymbol{\Sigma}_0) \propto |\boldsymbol{\Sigma}_0|^{-\frac{D+1}{2}}$;
- the prior for v_0 is set to a noninformative uniform prior:

  $\mathrm{p}(v_0) \propto$ constant.

The $\boldsymbol{\mu}_s$'s can be integrated out of the model (Marrelec et al., 2006b); the first two parts of the model are then replaced by a data likelihood of

$$\mathrm{p}(\boldsymbol{y}_s|\boldsymbol{\Sigma}_s) \propto |\boldsymbol{\Sigma}_s|^{-\frac{T-1}{2}} \exp\left[-\frac{1}{2}\mathrm{tr}(\boldsymbol{S}_s\boldsymbol{\Sigma}_s^{-1})\right],$$

with

$$\boldsymbol{S}_s = \sum_{t=1}^{T}(\boldsymbol{y}_{s,t} - \overline{\boldsymbol{y}_{s,t}})(\boldsymbol{y}_{s,t} - \overline{\boldsymbol{y}_{s,t}})^{\mathrm{t}},$$

proportional to the sample covariance matrix of subject s. Since the method used performs Gibbs sampling (Marrelec et al., 2006b), we must calculate the conditional distribution of each model parameter given to all others:

- for each subject s, $s = 1, \ldots, S$, we have for $\boldsymbol{\Sigma}_s|\text{rest}$:

$$\begin{aligned}\mathrm{p}(\boldsymbol{\Sigma}_s|\text{rest}) &\propto \mathrm{p}(\boldsymbol{y}_s|\boldsymbol{\Sigma}_s)\cdot\mathrm{p}(\boldsymbol{\Sigma}_s|\boldsymbol{\Sigma}_0, v_0)\\ &\propto |\boldsymbol{\Sigma}_s|^{-\frac{(T-1)+v_0+N+1}{2}}\exp\left\{-\frac{1}{2}\mathrm{tr}\left[(\boldsymbol{S}_s+\boldsymbol{\Sigma}_0)\boldsymbol{\Sigma}_s^{-1}\right]\right\},\end{aligned}$$

i.e.,

$$(\boldsymbol{\Sigma}_s|\text{rest}) \sim \text{Inv-Wishart}_{(T-1)+v_0}\left([\boldsymbol{S}_s+\boldsymbol{\Sigma}_0]^{-1}\right);$$

- for the group covariance matrix, $\boldsymbol{\Sigma}_0|\text{rest}$:

$$\begin{aligned}\mathrm{p}(\boldsymbol{\Sigma}_0|\text{rest}) &\propto \mathrm{p}(\boldsymbol{\Sigma}_0)\cdot\prod_{s=1}^{S}\mathrm{p}(\boldsymbol{\Sigma}_s|\boldsymbol{\Sigma}_0, v_0)\\ &\propto |\boldsymbol{\Sigma}_0|^{\frac{Sv_0-(N+1)}{2}}\exp\left\{-\frac{1}{2}\mathrm{tr}\left[\boldsymbol{\Sigma}_0\left(\sum_{s=1}^{S}\boldsymbol{\Sigma}_s^{-1}\right)\right]\right\},\end{aligned}$$

i.e.,

$$(\boldsymbol{\Sigma}_0|\text{rest}) \sim \text{Wishart}_{Sv_0}\left(\left[\sum_{s=1}^{S}\boldsymbol{\Sigma}_s^{-1}\right]^{-1}\right);$$

- as to $v_0|\text{rest}$:

$$\mathrm{p}(v_0|\text{rest}) \propto \mathrm{p}(\boldsymbol{\Sigma}_s|\boldsymbol{\Sigma}_0, v_0)\cdot\mathrm{p}(v_0) \propto \prod_{s=1}^{S}\text{Inv-Wishart}_{v_0}(\boldsymbol{\Sigma}_0;\boldsymbol{\Sigma}_s),$$

where $\text{Inv-Wishart}_{v_0}(\boldsymbol{\Sigma}_0;\boldsymbol{\Sigma}_s)$ stands for the value of the inverse Wishart distribution with degree of freedom v_0 and scale matrix $\boldsymbol{\Sigma}_0$ calculated at point $\boldsymbol{\Sigma}_s$.

We then run Gibbs sampling on the model to propose a numerical approximation of $\mathrm{p}(\boldsymbol{\Sigma}_0|\boldsymbol{y})$ (Ruanaidh and Fitzgerald, 1996; Gelman et al., 1998) and successively sample each variable given the set of remaining variables. $\boldsymbol{\Sigma}_s|\text{rest}$ and $\boldsymbol{\Sigma}_0|\text{rest}$ can be sampled directly from their conditional distributions. As to $v_0|\text{rest}$, a sample is obtained from a discrete approximation of this unidimensional distribution calculated over a finite grid. To allow for burn-in effect, we discard the first half of the samples and only keep the second half for consideration, that we note $(\boldsymbol{\Sigma}_0^{[l]})$, $l = 1, \ldots, L$. It is then possible to use Eqs. (9)–(11) to obtain samples for the various integrations of interest.

References

Achard, S., Salvador, R., Whitcher, B., Suckling, J., Bullmore, E., 2006. A resilient, low-frequency, small world human brain functional network with highly connected association cortical hubs. The Journal of Neuroscience 26, 63–72.

Anderson, T.W., 1958. An Introduction to Multivariate Statistical Analysis. Wiley Publications in Statistics. John Wiley and Sons, New York.

Bellec, P., Perlbarg, V., Jbabdi, S., Pélégrini-Issac, M., Anton, J.-L., Doyon, J., Benali, H., 2006. Identification of large-scale networks in the brain using fMRI. NeuroImage 29, 1231–1243.

Buonomano, D.V., Merzenich, M.M., 1998. Cortical plasticity: from synapses to maps. Annual Review of Neuroscience 21, 149–186.

Calautti, C., Baron, J.-C., 2003. Functional neuroimaging studies of motor recovery after stroke in adults. Stroke 34, 1553–1566.

Chen, W., Ogawa, S., 1999. Principles of BOLD functional MRI. In: Moonen, C., Bandettini, P. (Eds.), Functional MRI. Springer, Berlin, pp. 103–113.

Chialvo, D.R., 2004. Critical brain networks. Physica A: Statistical Mechanics and its Applications 340, 756–765.

Cover, T.M., Thomas, J.A., 1991. Elements of Information Theory. In: Wiley Series in Telecommunications and Signal Processing. Wiley.

Cramer, S.C., Nelles, G., Benson, R.R., Kaplan, J.D., Parker, R.A., Wong, K.K., Kennedy, D.N., Finklestein, S.P., Rosen, B.R., 1997. A functional MRI study of subjects recovered from hemiparetic stroke. Stroke 28, 2518–2527.

Dodel, S., Golestani, N., Pallier, C., El Kouby, V., Le Bihan, D., Poline, J.-B., 2005. Condition-dependent functional connectivity: syntax network in bilinguals. Philosophical Transactions of the Royal Society of London. Series B, Biological Sciences 360, 921–935.

Duffau, H., 2001. Acute functional reorganisation of the human motor cortex during resection of central lesions: a study using intraoperative brain mapping. Journal of Neurology, Neurosurgery, and Psychiatry 70, 506–513.

Duffau, H., 2005. Lessons from brain mapping in surgery for low grade glioma: insight into associations between tumour and brain plasticity. Lancet Neurology 4, 476–486.

Duffau, H., Capelle, L., Denvil, D., Sichez, N., Gatignol, P., Lopes, M., Mitchell, M.C., Sichez, J.P., Effenterre, R.V., 2003. Functional recovery after surgical resection of low-grade gliomas in eloquent

brain: hypothesis of brain compensation. Journal of Neurology, Neurosurgery, and Psychiatry 74, 901–907.

Fandino, J., Kollias, S.S., Wieser, H.G., Valavanis, A., Yonekawa, Y., 1999. Intraoperative validation of functional magnetic resonance imaging and cortical reorganization patterns in patients with brain tumors involving the primary motor cortex. Journal of Neurosurgery 91, 238–250.

Fontaine, D., Capelle, L., Duffau, H., 2002. Somatotopy of the supplementary motor area: evidence from correlation of the extent of surgical resection with the clinical patterns of deficit. Neurosurgery 50, 297–303.

Foucher, J.R., Vidailhet, P., Chanraud, S., Gounot, D., Grucker, D., Pins, D., Damsa, C., Danion, J.-M., 2005. Functional integration in schizophrenia: too little or too much? preliminary results on fMRI data. NeuroImage 26, 374–388.

Friston, K.J., 1994. Functional and effective connectivity in neuroimaging: a synthesis. Human Brain Mapping 2, 56–78.

Friston, K.J., Frith, C.D., Frackowiak, R.S.J., 1993a. Time-dependent changes in effective connectivity measured with PET. Human Brain Mapping 1, 69–79.

Friston, K.J., Frith, C.D., Liddle, P.F., Frackowiak, R.S.J., 1993b. Functional connectivity: the principal component analysis of large (PET) data sets. Journal of Cerebral Blood Flow and Metabolism 13, 5–14.

Gelman, A., Carlin, J.B., Stern, H.S., Rubin, D.B., 1998. Bayesian Data Analysis. Texts in Statistical Science. Chapman & Hall, London.

Hebb, D.O., 1949. The Organization of Behavior: A Neurophysiological Theory. Wiley, New York.

Holodny, A.I., Schulder, M., Ybasco, A., 2002. Translocation of Broca's area to the contralateral hemisphere as the result of the growth of a left inferior frontal glioma. Journal of Computer Assisted Tomography 26, 941–943.

Horwitz, B., 2003. The elusive concept of brain connectivity. NeuroImage 19, 466–470.

Horwitz, B., Poeppel, D., 2002. How can EEG/MEG and fMRI/PET data be combined? Human Brain Mapping 17, 1–3.

Huettel, S.A., Song, A.W., McCarthy, G., 2004. Functional Magnetic Resonance Imaging. Sinauer, Sunderland.

Jaynes, E.T., 2003. Probability Theory: The Logic of Science. In: Principles and Elementary Applications, vol. I. Cambridge University Press, Cambridge.

Jiang, T., He, Y., Zang, Y., Weng, X., 2004. Modulation of functional connectivity during the resting state and the motor task. Human Brain Mapping 22, 63–71.

Krainik, A., Duffau, H., Capelle, L., Cornu, P., Boch, A.-L., Mangin, J.-F., Bihan, D.L., Marsault, C., Chiras, J., Lehéricy, S., 2004. Role of the healthy hemisphere in recovery after resection of the supplementary motor area. Neurology 62, 1323–1332.

Krainik, A., Lehéricy, S., Duffau, H., Vlaicu, M., Poupon, F., Capelle, L., Cornu, P., Clemenceau, S., Sahel, M., Valery, C.-A., Boch, A.-L., Mangin, J.-F., Bihan, D.L., Marsault, C., 2001. Role of the supplementary motor area in motor deficit following medial frontal lobe surgery. Neurology 57, 871–878.

Kullback, S., 1968. Information Theory and Statistics. Dover, Mineola, NY.

Lee, L., Harrison, L.M., Mechelli, A., 2003. The functional brain connectivity workshop: report and commentary. Network: Computation in Neural Systems 14, R1–R15.

MacKay, D.J.C., 2003. Information Theory, Inference, and Learning Algorithms. Cambridge University Press, Cambridge.

Marrelec, G., Daunizeau, J., Pélégrini-Issac, M., Doyon, J., Benali, H., 2005. Conditional correlation as a measure of mediated interactivity in fMRI and MEG/EEG. IEEE Transactions on Signal Processing 53, 3503–3516.

Marrelec, G., Bellec, P., Benali, H., 2006a. Exploring large-scale brain networks. Journal of Physiology, Paris 100, 171–181.

Marrelec, G., Krainik, A., Duffau, H., Pélégrini-Issac, M., Lehéricy, S., Doyon, J., Benali, H., 2006b. Partial correlation for functional brain interactivity investigation in functional MRI. NeuroImage 32, 228–237.

McIntosh, A.R., Gonzalez-Lima, F., 1994. Structural equation modeling and its application to network analysis of functional brain imaging. Human Brain Mapping 2, 2–22.

Murase, N., Duque, J., Mazzochio, R., Cohen, L.G., 2004. Influence of interhemispheric interactions on motor function in chronic stroke. Annals of Neurology 55, 400–409.

Naidich, T.P., Hof, P.R., Yousry, T.A.Y., 2001. The motor cortex: anatomic substrates of function. Neuroimaging Clinics of North America 11, 171–193.

Passingham, R.E., Stephan, K.E., Kötter, R., 2002. The anatomical basis of functional localization in the cortex. Nature Reviews Neuroscience 3, 606–616.

Rijntjes, M., Weiller, C., 2002. Recovery of motor and language abilities after stroke: the contribution of functional imaging. Progress in Neurobiology 66, 109–122.

Roland, P.E., Zilles, K., 1998. Structural divisions and functional fields in the human cerebral cortex. Brain Research Reviews 26, 87–105.

Ruanaidh, J.J.K.O., Fitzgerald, W.J., 1996. Numerical Bayesian Methods Applied to Signal Processing. Statistics and Computing. Springer, New York.

Salvador, R., Suckling, J., Coleman, M., Pickard, J.D., Menon, D., Bullmore, E., 2005. Neurophysiological architecture of functional magnetic resonance images of human brain. Cerebral Cortex 34, 387–413.

Shannon, C.E., 1948. A mathematical theory of communication. The Bell System Technical Journal 27, 379–423, 623–665.

Sporns, O., Chialvo, D.R., Kaiser, M., Hilgetag, C.C., 2004. Organization, development and function of complex brain networks. Trends in Cognitive Sciences 8, 418–425.

Sporns, O., Tononi, G., Edelman, G.M., 2000. Connectivity and complexity: the relationship between neuroanatomy and brain dynamics. Neural Networks 13, 909–922.

Stepanyants, A., Chklovskii, D.B., 2005. Neurogeometry and potential synaptic connectivity. Trends in Neurosciences 28, 387–394.

Stone, J.V., Kötter, R., 2002. Making connections about brain connectivity. Trends in Cognitive Sciences 6, 327–328.

Studený, M., Vejnarová, J., 1998. The multiinformation function as a tool for measuring stochastic dependence. In: Jordan, M.I. (Ed.), Learning in Graphical Models. Kluwer, Dordrecht, pp. 261–298.

Talairach, J., Tournoux, P., 1988. Co-Planar Stereotaxic Atlas of the Human Brain. Georg Thieme, Stuttgart.

Thiel, A., Habedank, B., Winhuisen, L., Herholz, K., Kessler, J., Haupt, W.F., Heiss, W.-D., 2005. Essential language function of the right hemisphere in brain tumor patients. Annals of Neurology 57, 128–131.

Thiel, A., Herholz, K., Koyuncu, A., Ghaemi, M., Kracht, L.W., Habedank, B., Heiss, W.-D., 2001. Plasticity of language network in patients with brain tumors: a positron emission tomography activation study. Annals of Neurology 50, 620–629.

Toni, I., Rowe, J., Stephan, K.E., Passingham, R.E., 2002. Changes of cortico-striatal effective connectivity during visuomotor learning. Cerebral Cortex 12, 1040–1047.

Tononi, G., Edelman, G.M., Sporns, O., 1998a. Complexity and coherence: integrating information in the brain. Trends in Cognitive Sciences 2, 474–484.

Tononi, G., McIntosh, A.R., Russel, P., Edelman, G.M., 1998b. Functional clustering: identifying strongly interactive brain regions in neuroimaging data. NeuroImage 7, 133–149.

Tononi, G., Sporns, O., Edelman, G.M., 1994. A measure for brain complexity: relating functional segregation and integration in the nervous system. Proceedings of the National Academy of Sciences of the United States of America 91, 5033–5037.

Varela, F.J., Lachaux, J.-P., Rodriguez, E., Martinerie, J., 2001. The brainweb: phase synchronization and large-scale integration. Nature Reviews Neuroscience 2, 229–239.

Whittaker, J., 1990. Graphical Models in Applied Multivariate Statistics. John Wiley and Sons, Chichester.

Wunderlich, G., Knorr, U., Herzog, H., Kiwit, J.C.W., Freund, H.-J., Seitz, R.J., 1998. Precentral glioma location determines the displacement of cortical hand representation. Neurosurgery 42, 18–27.

Zeki, S., Shipp, S., 1988. The functional logic of cortical connections. Nature 335, 311–317.